CEAS Aeronautical Journal (2022) 13:861–876
https://doi.org/10.1007/s13272-022-00603-4

ORIGINAL PAPER

Integration of propelled yaw control on wing tips: a practical approach to the Icaré solar-powered glider

Johannes Schneider[1] · Michael Frangenberg[2] · Stefan Notter[2] · Werner Scholz[3] · Walter Fichter[2] · Andreas Strohmayer[1]

Received: 8 March 2021 / Revised: 23 May 2022 / Accepted: 4 July 2022 / Published online: 6 September 2022

Abstract
In this practical approach to distributed propulsion, the solar-powered manned motorglider icaré 2 has been used as a testbed for wingtip propulsion. The large wingspan and slow cruising speed of icaré 2 are highly suitable to assess the influence and potential of propellers at the wingtips for yaw control. The paper describes the work of a multidisciplinary team consisting of researchers, engineers, pilots and students, starting from the initial idea to use propellers at the wingtips of icaré 2 up to the actual flight test campaign. First, the design and development of the modular wingtip pods are described to house the propeller, electric motor, battery and further sensors and control systems. Furthermore, the modifications required for integrating the wingtip pods on the aircraft itself are outlined and the electrical and mechanical interfaces are defined and described. To obtain a permit to fly for the new configuration of the aircraft, several tests on system level of the wingtip pods needed to be conducted and documented for the authorities. Finally, the flight test campaigns carried out to date are outlined and described including the planning, lessons learned and results.

Keywords Wingtip propulsion · Distributed electric propulsion · Electric aircraft

1 Background: distributed electric propulsion

Recently, distributed electric propulsion (DEP) has been investigated to a great extent by many research facilities and aircraft OEM's (Original Equipment Manufacturer). Due to their fairly high power to weight/volume ratio and reduced complexity, electric motors make it possible to place the propulsion systems almost everywhere and in any size on the aircraft. A smart layout of the propulsive system on the aircraft can contribute in several ways to the environmental impact of the aircraft. Therefore, DEP is one of the most promising technologies to achieve the ambitious goals set by the European Union to make air transportation more environmentally friendly [1].

✉ Johannes Schneider
Johannes.schneider@ifb.uni-stuttgart.de

[1] Institute of Aircraft Design, University of Stuttgart, Stuttgart, Germany

[2] Institute of Flight Mechanics and Control, University of Stuttgart, Stuttgart, Germany

[3] SFL GmbH, Stuttgart, Germany

By distributing the power over the whole wing, improvements in safety and redundancy can be achieved as well as a reduction in propeller loading. This leads to increased efficiency and further decreased noise emissions [2]. Moreover, enhanced maneuvering capabilities are achieved as well as improved crosswind capabilities [3]. In addition, the maneuvering capabilities of the propulsion system allow for a reduced size of the vertical tailplane and therefore reduced drag [3].

As shown in Fig. 1, the wingtips and empennage can be used to distribute the propulsion systems in a smart way,

Fig. 1 Aircraft concept with distributed electric propulsion—The Hybird [4]

exploiting various aerodynamic and structural synergy effects and leading to fairly efficient aircraft concepts. The lift distribution of the wing and the free stream velocity of the air can be influenced by the propulsion system to increase the overall lift. This allows a reduction of the wing area and, therefore, results in less mass and parasitic drag [5]. The distribution of the electric motors along the wing counteracts the spanwise lift force and can lead to a reduction in wing bending momentum and a further improvement in flutter and aeroelasticity characteristics.

Wingtip propellers play a main role in the DEP philosophy and can be seen as active winglets, supporting or even replacing a vertical tailplane. The wingtip propellers are mounted in such a way that the interference with the local vortex flow around the wingtips creates synergetic benefits, reducing drag and increasing efficiency [5]. Furthermore, the reduced lateral flow leads to an increase in local lift produced at the wingtips. Distributed electric propulsion and wingtip propellers are capable of decreasing the need for traditional control surfaces due to the usage of differential thrust and increased tolerance with respect to engine-out or propulsor-out failure cases [6].

2 ICARÉ 2—the perfect testbed

2.1 Icaré system overview and description

The icaré 2 (Fig. 2) is a solar-powered one-seater motorized sailplane designed and developed in 1994 by the department of aerospace engineering of the University of Stuttgart. At that time and even nowadays icaré 2 is still a unique aircraft. The large wing and empennage are covered with photovoltaic solar collectors. The aircraft's main design driver was to install enough surface for photovoltaic cells to be able to fly an unlimited amount of time during a sunny day. The wing and fuselage are made from carbon fiber composites. The electric motor with a large two blade foldable propeller sits at the rear top of the vertical tailplane in a pusher configuration.

In the year 1996, the icaré 2 won the Berblinger Competition. From then until now, several modifications of the systems and the aircraft configuration itself have been successfully implemented and flight tested. At the moment, the aircraft can be used in two different configurations:

1. *icaré 2 xxl* (Fig. 3) with winglets
2. *icaré 2 wtp* (Fig. 4) with wingtip propellers, replacing the winglets

As a result of the continuous upgrades, the aircraft has become very reliable and obtained a set of highly integrated systems for data logging. The integrated 2.9kw/h lithium polymer batteries allow the aircraft to take off by itself and climb to an altitude of 1000 m above the ground without using the solar generator as an additional energy supply. Alternatively, icaré 2 can be towed to an adequate altitude, similar to conventional gliders.

As mentioned before, the aircraft has been used as a test bed and technology demonstrator for the University of Stuttgart for more than 20 years. The data acquisition systems integrated in the aircraft allow for comprehensive data logging. An air data boom, which protrudes from the fuselage nose, tracks the airspeed, angle of attack and the angle of sideslip. The deflection angles of horizontal tailplane, rudder and ailerons are tracked by potentiometers on the mechanical steering system. Moreover, the attitude and the flight path are tracked by a combination of an Inertial Measurement Unit (IMU) and GPS trackers. The energy, battery and propulsion management systems

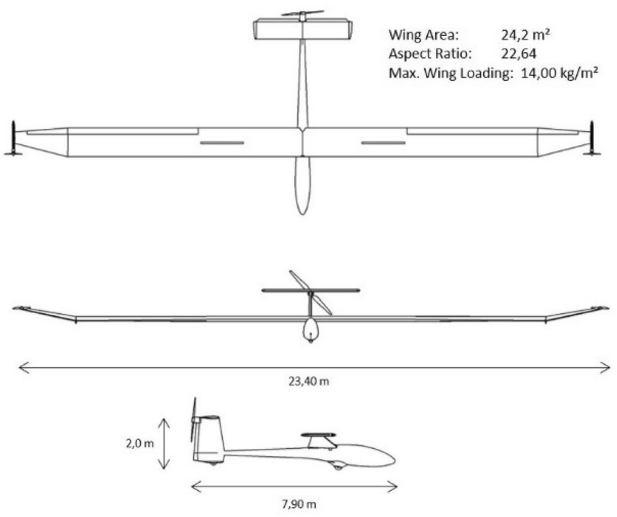

Fig. 2 Icaré 2 wtp three side view

Fig. 3 Icaré 2 xxl version with winglets

Fig. 4 Icaré 2 wtp version with wingtip propellers

store data throughout the flight. The measurands are voltage, temperatures, current, power, rounds per minute of the propeller, energy collected by the solar generator and energy needed throughout the flight by the propulsion system.

The testing of a propelled yaw control system benefits from the configuration of icaré 2. A maximum takeoff mass of 430 kg, together with a large wing span (23.4 m) and wing surface area (25.7 m^2) lead to a very low wing loading (16.3 kg/m^2), resulting in slow flying speeds and a high yaw moment of inertia. It has been even possible to use commercial off-the-shelf (COTS) components for the wing tip propulsion system. An aircraft with a higher wing loading and, therefore, higher speeds might need a special set of electric motors and propellers to be capable of achieving yaw control on a propelled wingtip system. This also would lead to a heavier battery for the yaw control system.

2.2 Flight performance

The flight performance of icaré 2 is as unique as the configuration. With an average cruising speed of 70 km/h and a v_{NE} of 90 km/h, it is quite slow. As mentioned before, the combination of efficient gliding abilities and an effective powertrain allows icaré 2 to fly for an unlimited time. On a sunny day, the photovoltaic system and the solar generator provide 2.9 kW of electric power, which is enough to maintain horizontal flight and to charge the battery. The low wing loading is also a benefit while using thermal activity to climb and gain altitude. Maneuvering icaré 2 when gliding sometimes is a bit tricky, especially in the yaw axes due to the high momentum of inertia and a rather small vertical tail volume.

2.3 Preparations for integration

As stated before, the aircraft is already fully equipped with systems for tracking and logging attitude, track and control surface inputs. There is an existing structural interface for winglets at the wingtips. This interface is used to attach the wingtip pods which house the battery, power distribution systems, control systems and the electric motor of the wingtip propulsion. Consequently, the mechanical interface between the wingtip propulsion and the wing does not require any adjustments to the existing structure. The winglets were removed and the pods, making use of the same interface, can be attached.

For the data link between the pods and the cockpit, a network cable has been attached on the trailing edge of the wing. This datalink is used to command and monitor the wingtip pods. The cockpit was upgraded with several modifications. The use of the propelled yaw control system on the wingtips is only temporary. Therefore, the functions to command and monitor them were not implemented in the existing software code of the aircraft, which monitors the solar generator and main propulsion system, but remain stand alone. This decision was also made due to safety reasons. Furthermore, all components can be removed easily in case the aircraft is needed in the standard configuration for a different mission.

It was necessary to integrate a couple of new systems in the cockpit to ensure overall aircraft safety, mainly due to the significant increase of propulsive power with the wingtip propellers. Furthermore, a flexible and adaptable command and control system is needed to have an effective flight test campaign. The software code for the command and monitor functions has been implemented on a separate computer (the "magic box", Fig. 5). It is possible to attach and detach the magic box very quickly in the cockpit to edit the software code in the labs after a flight test campaign.

An additional display (Fig. 6) shows all the information necessary to operate the wingtip propellers. It is within good reach for the pilot to skip through the different pages

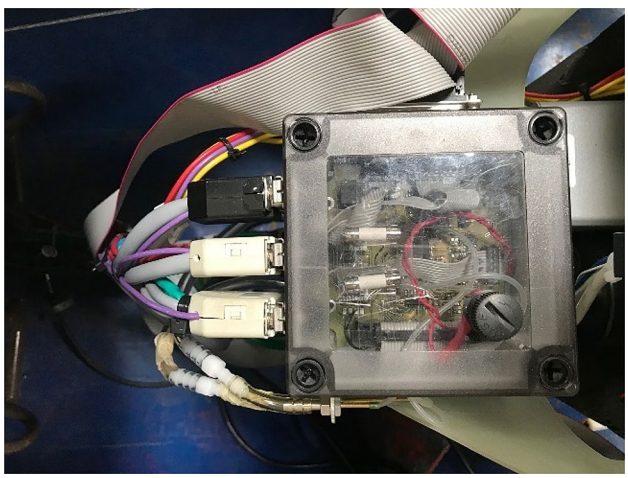

Fig. 5 The "magic box"—control unit for wingtip propellers

Fig. 6 Wingtip propulsion control display

of information. The display including the bracket can be attached and detached easily to enter the cockpit and to use the icaré 2 in standard configuration.

For both wing tip pods, the following parameters are displayed individually:

- propeller speed in rpm,
- voltage, current and power of the motor,
- battery voltage and temperature,
- temperature of the motor controller,
- wingtip propulsor control

Finally, an additional sidestick has been integrated so that the pilot can easily reach it (Fig. 7).

The sidestick, similar to the ones used by remote controls of model aircraft, controls the power/thrust provided by the wingtip propellers. When pushed forward or backwards, the

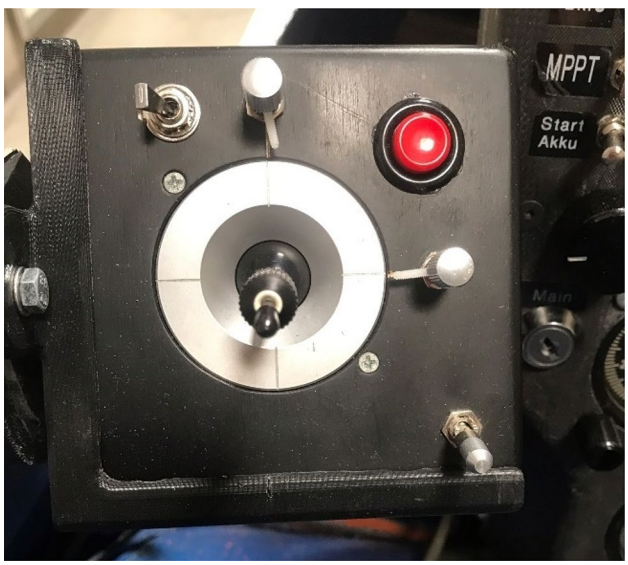

Fig. 7 Sidestick to control wingtip propellers

Fig. 8 Modified cockpit layout of the icaré wtp

power is set collectively on both wingtip propellers. The sidestick stays in the position set by the pilot. By pushing the sidestick to the sides, the power/thrust on each wingtip can be set individually by adding power to the electric motor based on the pre-set collective power setting. When using differential power levels, the sidestick always returns to the neutral middle position by itself. As can be seen in Fig. 7, there are also several buttons on the sidestick. They are used to switch between different control modes, which are defined in Sect. 5 of this paper, and to adjust the command sensitivity of the sidestick in relation to the output signal from a linear to a more exponential performance.

A runaway of the wingtip propellers might lead to a hazardous failure in terms of yaw control. Therefore, a kill switch button has been installed in the cockpit, which triggers a relay in the wingtip pods to cut-off the electronic speed controller of the battery. The modified cockpit layout for the icaré wtp variant can be seen in Fig. 8.

3 Design and development of modular wingtip pods

3.1 The necessary modularity

Currently manned aircraft using wingtip propellers for yaw control do not exist. Therefore, there is a lack of

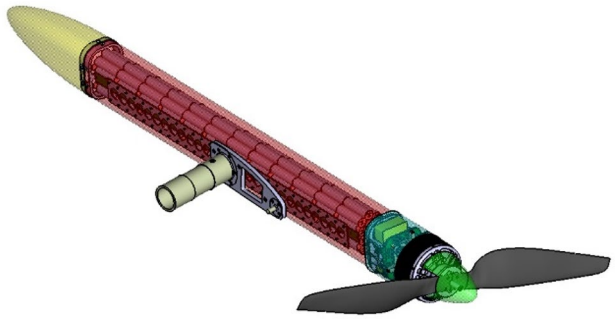

Fig. 9 Wingtip pod for propelled yaw control

experience about what position and configuration will work best. As previously laid out, no major system and structure will be changed on icaré 2 and the aircraft will be ready for flying in its standard configuration at any time. A pod which houses the system and components has been developed (Fig. 9). This makes it easy to remove the system completely from the wing. The only item which needs to be attached is the command and control cable and a safety pin to prevent the wingtip pods from detaching.

The pods can be turned around to switch between a pusher and tractor propeller configuration and moreover, they are designed to vary the position of the x-axis by changing the mounting spot on the wing connector. This allows different distances between the propeller and the wings' trailing edge and leading edge, respectively.

The system is capable of mounting different propellers on the wingtip pods. As stated earlier, COTS components and the introduced safety features will be capable of measuring and validating a propelled yaw control system via wingtip propellers on the icaré. This makes it relatively cheap and easy to test different types of propellers such as multiblade propellers, foldable propellers, and propellers with different diameters and pitch.

For an adequate validation of the capability of propelled yaw control, the system offers different semi-automatic and automatic control modes for the pilot. Buttons and switches integrated on the sidestick allow to change the control modes in flight.

3.2 Sizing of components

The pods are designed in a frame and skin construction, manufactured from carbon fibres and foam, consisting of a left and right side which can be separated (Fig. 10). The battery brackets (c.) (e.) act as frames when the pod is closed.

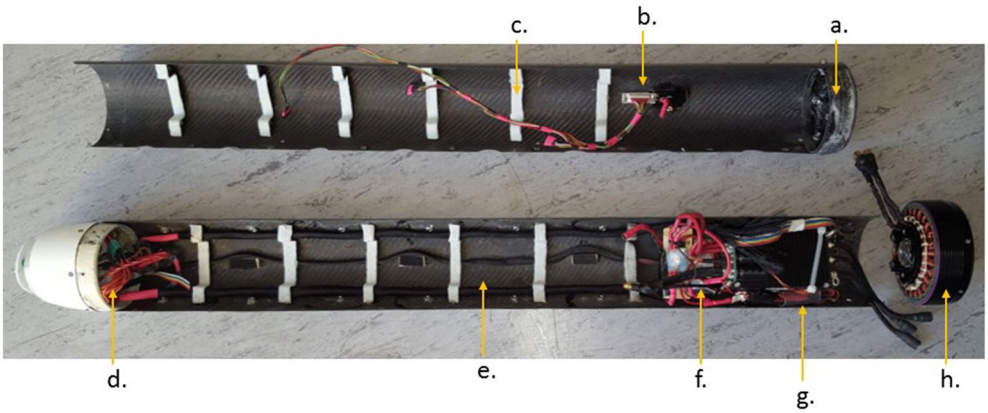

Fig. 10 Icaré wingtip pod components

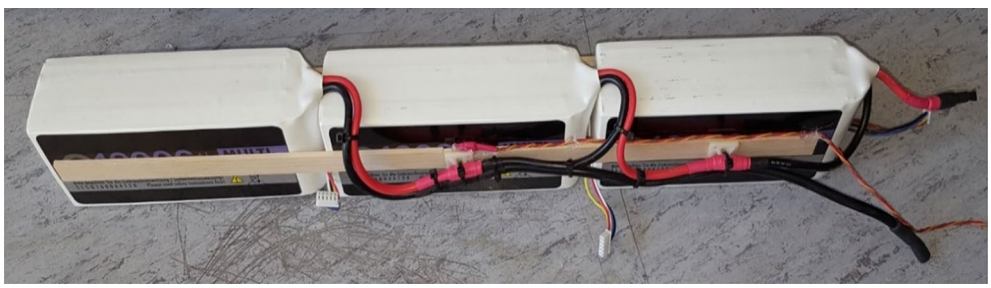

Fig. 11 Battery pack of the wingtip propulsion system

Furthermore, a frame (a.) for the motor (h.) and a frame (d.) for switches and the electric distribution and control board has been developed and integrated.

The electric motor sets the basis for all other electric components, in particular the motor controller (f.), the power sensors (g.) and the batteries (Fig. 11), since they have to deal with its current voltage and power demand.

The electric motor of the wingtip pod is the main design driver to size the system for propelled yaw control. The yaw momentum $M_{z_{wtp}}$ which can be generated by the thrust N_{wtp} of the wingtip propellers shall not exceed the yawing-moment-due-to-rudder derivative $C_{n_{\delta_r}}$ on the vertical tailplane. Nevertheless both control forces needs to be in the same range to be effective and to have a similar control behavior. Therefore, the rudder control power $C_{n_{\delta_r}}$ in cruise speed around the center of gravity is determined using the theoretical approach according to DATCOM [8] as followed:

$$C_{n_{\delta_r}} = -\frac{C_{y_{\delta_r}}\left(r_v \times \cos\alpha + z_v \sin\alpha\right)}{b}. \tag{1}$$

The yaw momentum on the icaré is generated by moving a rudder, as part of the symmetrical airfoil of the vertical tailplane, on one or the other side. Due to the very low wing loading of 15 kg/m^2, the angle of attack α is rather low. Leading to the simplified equation for the rudder control power:

$$C_{n_{\delta_r}} = \frac{-C_{y_{\delta_r}} \times r_v}{b} \tag{2}$$

with r_v the distance between the center of gravity (CG) and the aerodynamic center of the vertical tail plane ($AC_{tailplane}$). b the wingspan and $C_{y_{\delta_r}}$ the side-force-due-to-rudder derivative.

During yawing, the vertical fin experiences a lateral flow which changes the angle of attack of the fin. Moreover, the lateral movement of the fin increases the drag. Both effects counteract $C_{n_{\delta_r}}$ but are neglected due to the slow yawing speed and in general slow cruising speeds of the icaré. In the later explained aerodynamic analysis to determine the rudder control power, the effects on the flow of the vertical tailplane due to the aircraft movement around the vertical axis are also not considered.

The side-force-due-to-rudder derivative $C_{y_{\delta_r}}$ is also determined according to DATCOM [8].

$$C_{y_{\delta_r}} = \left(C_{L_{\alpha_v}}\right) \times \left(k' \times k_b\right) \times \left\{\frac{c_{l_\delta}}{\left(c_{l_\delta}\right)_{theory}}\right\} \times \left(c_{l_\delta}\right)_{theory} \times \left(\frac{S_v}{S}\right).$$

The lift curve slope $C_{L_{\alpha_v}}$ at low mach numbers and moderate sweep angles can be estimated from Fig. 12 using the vertical tails' effective aspect ratio $A_{v_{eff}}$ which is determined with [7]:

$$\Lambda_{v_{\text{eff}}} = \frac{A_{v(f)}}{A_v} \times A_v \times \left\{1 + K_{vh} \times \left(\frac{Av_{(hf)}}{A_{v(f)}}\right) - 1\right\}.$$

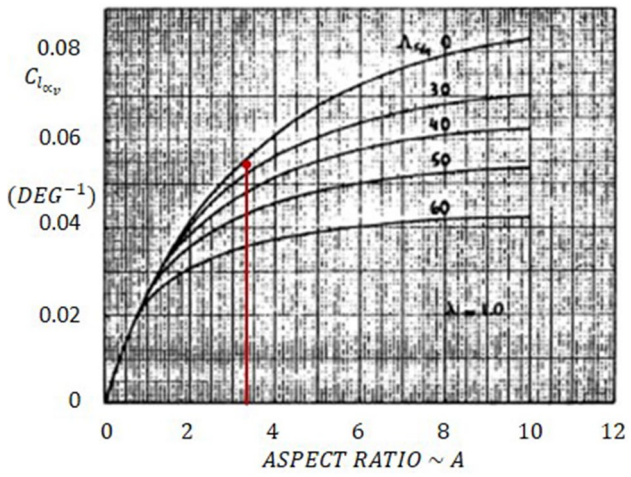

Fig. 12 Lift Curve Slope at low Mach Numbers and moderate sweep angles [7]

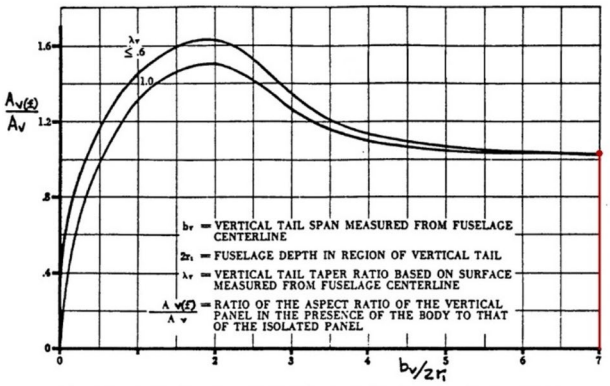

Fig. 13 Ratio of vertical tail aspect ratio in presence of fuselage to that of isolated tail [7]

The ratio of the vertical tail aspect ratio in presence of a fuselage to the aspect ratio of an isolated tail $\frac{A_{v(f)}}{A_v}$ can be found in Fig. 13 [7]. The factor K_{vh} which accounts for the

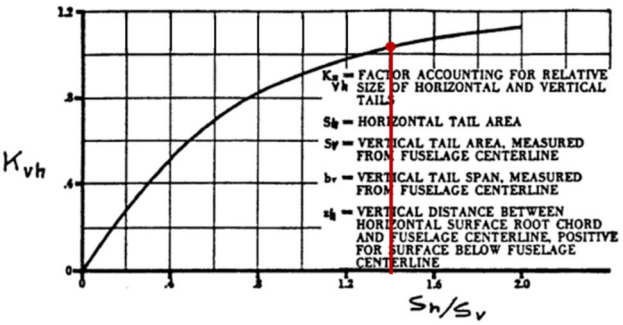

Fig. 14 Factor which accounts for relative size of horizontal and vertical tail [7]

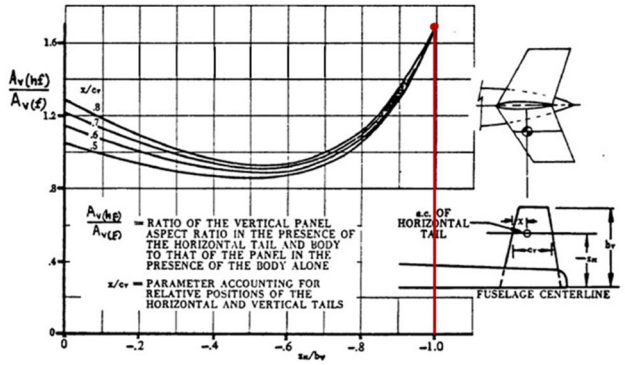

Fig. 15 Ratio of vertical tail aspect ratio [7]

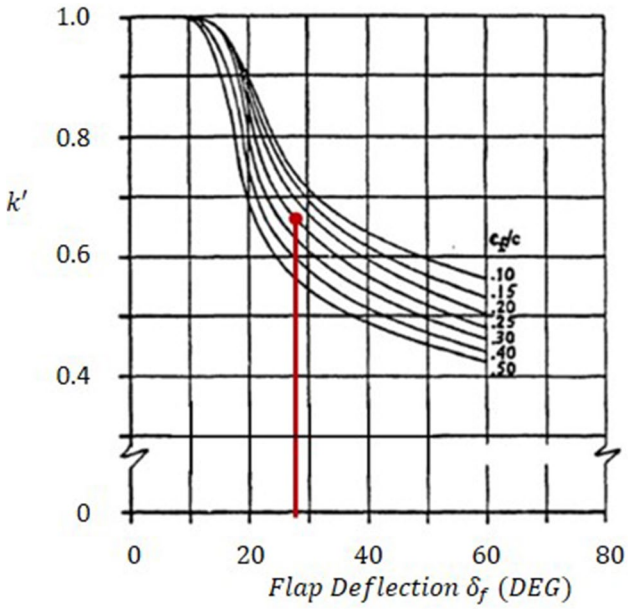

Fig. 16 Correction factor for nonlinear lift behavior of plain flaps [8]

relative size of the horizontal and vertical tail can be found in Fig. 14 [7].

Furthermore, the ratio of the vertical tail aspect ratio in presence of a fuselage and horizontal tail to that in presence of a fuselage alone $\left(\frac{Av_{(hf)}}{A_{v(f)}}\right)$ can be derived from Fig. 15.

The side-force-due-to-rudder-derivative determination methodology according to [8] requires to introduce the correction factor for nonlinear lift behavior of plain flaps k' and the flap span factor K_b. The two parameters can be estimated for the icaré from Figs. 16 and 17. The maximum deflection of the icaré rudder is $\delta_r = 27°$

The vertical tailplane of the icaré uses the Wortmann FX71-L-150/30 [8] airfoil with a maximum thickness of 15%. To derive the correction factor for plain flap lift

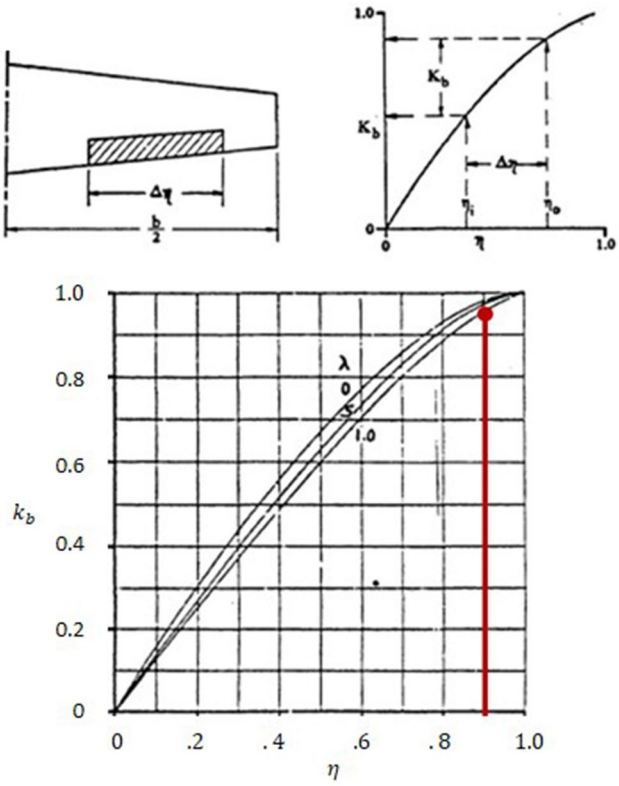

Fig. 17 Effects on flap span factor Kb [8]

$\left(c_{l_\delta}(c_{l_\delta})_{\text{theory}}\right)$ a look into the airfoils lift curve slope c_{l_α} is necessary. With Fig. 18, the correction factor can be derived.

The lift effectiveness of a plain flap $\left(c_{l_\delta}\right)_{\text{theory}}$ can be derived from Fig. 19.

Equation (2) now results in a maximum rudder power $C_{n_{\delta_r}}(27°) = 1492Nm$ in cruise. However, in actual flight operations, a $C_{n_{\delta_r}}(15°) = 874\text{Nm}$ is more applicable.

The determined values for the rudder power of the theoretical approach are verified using the surface vorticity

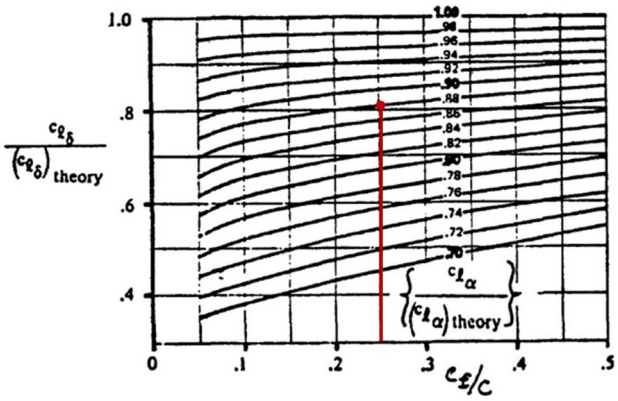

Fig. 18 Correction factor for plain flap lift [8]

flow solver FlightStream® [9]. The tool is used to directly ascertain the force of the rudder F_{r_y} in y-direction of the aircrafts coordinate system and the lift-coefficient C_{L_r} of the vertical tailplane at different rudder deflection angles.

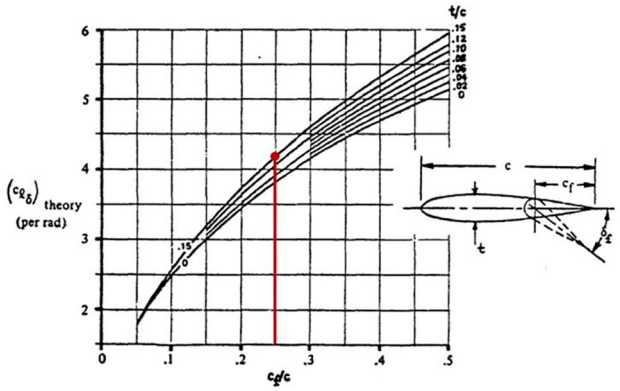

Fig. 19 Lift effectiveness of a plain flap [8]

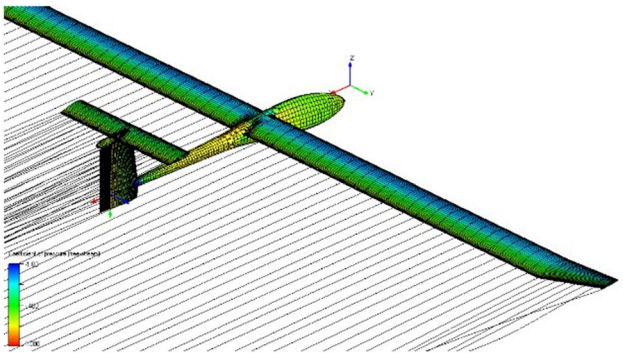

Fig. 20 Icaré reference simulation with FlightStream®

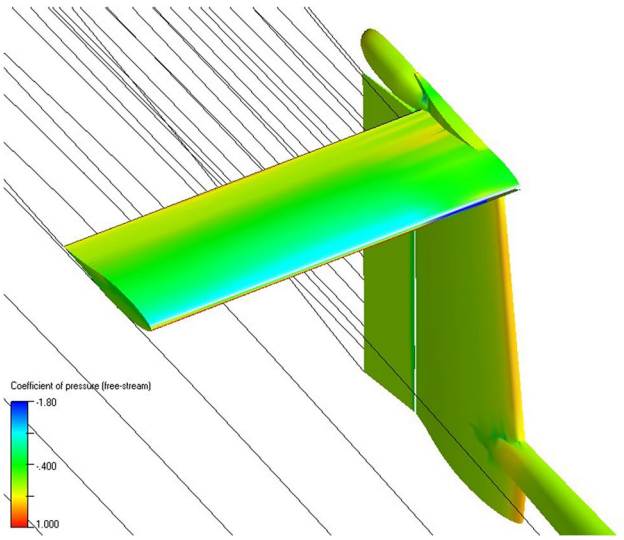

Fig. 21 Simulation with a rudder deflection of 5°

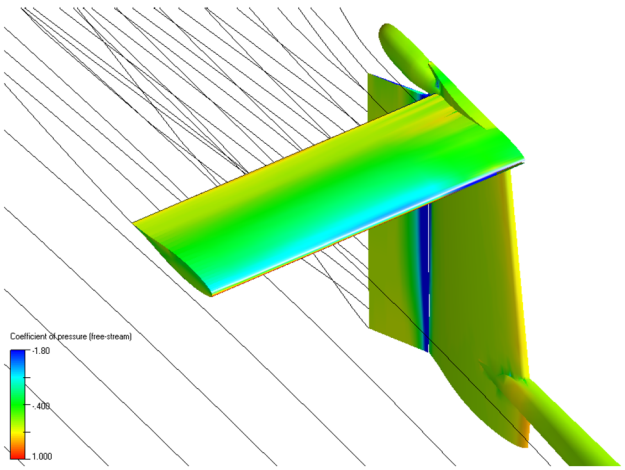

Fig. 22 Simulations with a rudder deflection of 20°

The solver is set up to simulate the flow at a $v_c = 22\frac{\text{m}}{\text{s}}$ and an angle of attack of $\alpha = 2°$.

As a reference and to check for a diverged solution the solver has been executed without a deflection angle of the rudder (Fig. 20).

In each following run the rudder deflection δ_r is increased by 5° from 0° to 27° (Fig. 21, 22).

The resulting forces F_{r_Y} and the yaw momentum M_z are stated in Table 1. The lever arm r_r ($\text{AC}_{\text{tailplane}}$–$CG$) has been measured a value of $r_r = 5{,}20$ m.

Again, in cruise flight a $\delta_r = 15°$ and the corresponding $M_z = 741\text{Nm}$ is more appropriate to use as a design baseline. Nevertheless, a value of $M_z = 1000\text{Nm}$ shall be the design momentum for the wtp system of the icaré. This has been chosen as the design point because with a relatively similar momentum M_z, which the wtp system and the rudder can apply, a similar behavior of the yawing in cruise flight is prognosed. This is more comfortable, hence safer, for the test pilot who knows the aircraft for 25 years. Moreover, in case of a one-sided motor runaway on the wing tip, the pilot is still able to counteract the design momentum of the wtp system with the full deflection of the rudder to prevent uncontrolled flight conditions.

Due to the higher lever arm $r_W = 11,70\text{m}$ of the wing compared to the empennage, a thrust $T_{\text{wtp}} = 85,4\text{N}$ equals the design yaw momentum for the wtp system.

Table 1 Rudder deflection simulation results

δ_r (°)	$F_{r_y}(N)$	M_z (Nm)
5	19	98,89308
10	81	419,1044
15	143	741,884
20	206	1069,068
25	270	1402,544
27	296	1538,0508

Fig. 23 Ground clearance analysis for icaré 2 wingtip propellers

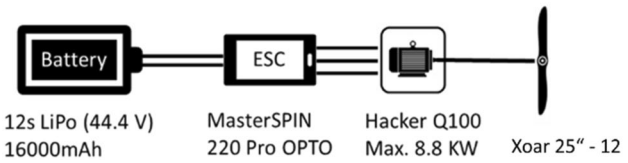

Fig. 25 Wingtip pods powertrain components

The T_{wtp} needed and the given cruise flight speed of the icaré is used to choose a suitable propeller. The ground clearance as a further requirement limits the propeller diameter to 0.73 m (Fig. 23).

Furthermore, it is necessary to have a clockwise turning propeller for the right wingtip and an anticlockwise turning propeller for the left wingtip. Therefore, a market search of COTS RC-Model fixed pitch propellers has been conducted. In this market, segment propellers with 25″ diameter are the tallest to find for all of the above stated requirements. Several propellers with different diameters, propeller-pitch and rotation speed have been investigated with the tool propcalc [10] which computes the performance data of propellers with a given geometry. The tool uses an algorithm developed by Helmut Schenk based on the momentum theory, blade element momentum theory and a database with experimental data [10]. The analysis results of the finally chosen propeller with 25″ diameter, 12″ pitch and a rotation speed of 5000 rpm are shown in Fig. 24. It can be seen that 12″ pitch is a suitable value since this propeller has an efficiency $\eta = 0,6$ and above for the flight speed range of the icaré (15–25 m/s). In addition, the achievable propeller thrust vs. flight speed is shown, which is mainly dependent on the propeller diameter. A rotation speed of 5000 rpm has been chosen as an empirical value considering the propeller tip speed to avoid compressibility effects and the ratio $\frac{v_{pitch,propeller}}{v_{cruise,icaré}}$ for the investigated propeller configuration. At 18 m/s, a thrust of 80 N is determined which is close to the design T_{wtp}, hence a suitable value.

From the determined power and rotation speed, the requirements for the electric motor can be derived. The Hacker® Q100 motor [11] and a 2 bladed 25″–12″ Xoar® wood propeller [12] was found to be suitable to reach the needed thrust levels, being at the upper end of COS/rc-model sport products. Brushless electric motors of this size have quite low kv-values (rpm/V), hence the voltage needs to be high to reach the rotational speed for the required thrust, hence the lithium polymer battery packs need to have a certain number of cells. This sets the requirements in terms of power, current and voltage for the motor controller (ESC—Electronic Speed Controller), cables and sensors. The following Fig. 25 specifies the compatible components of the power train in the wingtip pods which fulfill the determined and simulated design T_{wtp} thrust requirement.

3.3 Power distribution and control board

In the rear of the wingtip pods, a control board has been developed and mechanically integrated to control the wingtip yaw control system (Fig. 26). The mechanic switches at the rear end of the pod (Fig. 27) activate the power distribution and thus increase safety when handling the pods on

Fig. 24 PropCalc wtp propeller results

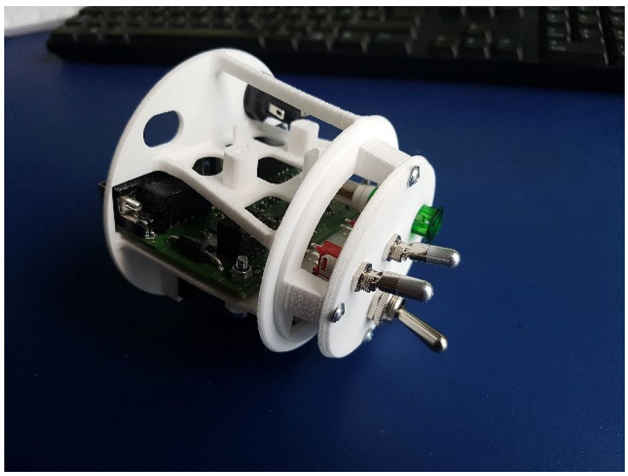

Fig. 26 Power distribution and control unit

Fig. 27 Activation switches

ground: switch S0 activates the 12 V power supply for data logging and transmitting, switch S1 preloads the capacitors of the motor controller to protect it from an overload when arming, and S2 finally arms the motor controller if the kill switch in the cockpit is set on, whereby the relay is open.

Two external connectors shown in Fig. 10b provide the data and control link and allow for charging and balancing the batteries.

3.4 Sensors and system

The test instrumentation is an integral part of the wingtip propeller system and consists of several microcontrollers:

a) 1 × sensorboard per pod for data acquisition (temperature, current, voltage, rounds per minute)
b) 1 × RS422 driver board per pod for data communication,
c) 1 × analog–digital converter board
d) 1 × onboard computer with GPS data (Global Positioning System), IMU data (Inertial Measurement Unit) and a memory card for storage.

The sensor boards in the pods, GPS, IMU and position sensors of the control surfaces record a wide variety of flight data and pass it on to the central onboard computer of icaré 2 to store it on an SD memory card.

All data have a time stamp on the respective microcontroller at the time of recording and another time stamp on the onboard computer at the time of saving. Figure 28 [13] shows a detailed sensor and control layout. An air data boom was attached to the aircraft to measure total pressure and static pressure as well as the angle of attack and angle of sideslip. For the test flights, comments on the test maneuvers are recorded by the pilot to take the "pilots feeling" into account.

4 Authorization requirements

4.1 Propellers as flight control systems

The icaré 2 is a motorized sailplane registered in Germany. Since the icaré 2 is an experimental aircraft it has no type certification and only gets a *VVZ* (*Vorläufige Verkehrszulassung* | engl.: Permit to Fly) on an annual basis after a

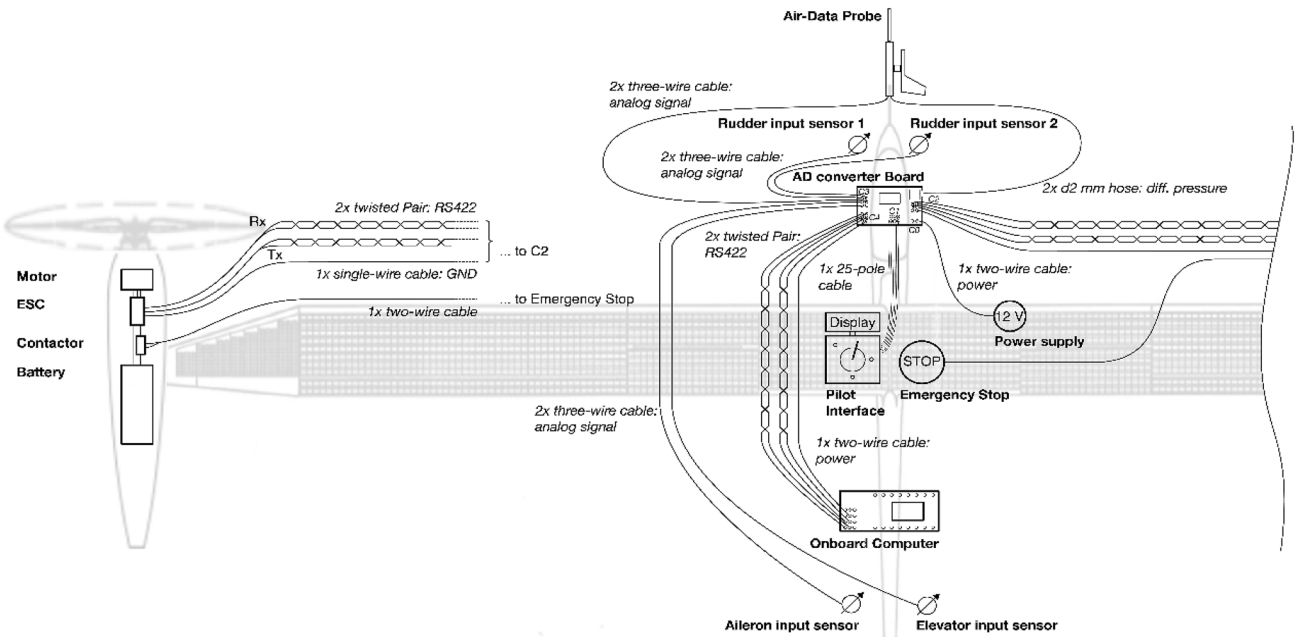

Fig. 28 Sensor and control Layout of icaré wtp

clearance certificate of a representative of the "LBA" (*Luftfahrtbundesamt* | engl.: Federal Aviation Office). All major changes on the aircraft need to be communicated to the LBA and clarified individually. The wingtip pods with the motor and propeller are not declared as propulsion systems but as (primary) flight control systems, so with respect to the aircraft category the icaré 2 wtp remains a single-engine aircraft.

4.2 Windmill tests

When using non-folding propeller blades on the wingtip pods they will start to windmill as soon as the power supply is cut-off or the system is not in use. Windmilling propellers would induce an electric voltage in the motor, motor controllers and batteries. To receive a permit to fly with wingtip propellers, it was required to prove that windmilling and the induced voltage are not critical for the system components. Therefore, windmilling tests have been conducted in a windtunnel as a safe environment. The rotational speed of the propeller has been measured during windmilling and found not to exceed 3000 rpm. In a second, more cost efficient test set up, the "longterm" impact of the induced voltage due to a windmilling propeller has been evaluated. The test stand is shown in Fig. 29. It is divided into the active side (right) and the passive side (left). The motor on the active side is controlled and electrically propelled. The various engine speeds are set and maintained using an RC control system. A magnetic sensor on the shaft balancing joint measures the rotational speed. The motor controller on the active side is also equipped with two temperature sensors. The passive side is identical to the active side and consists of a motor, controller and batteries. However, the passive side was not directly controlled and electrically driven during the test. The propeller speed that causes windmilling is transmitted from the electrically driven active side to the passive side by a shaft.

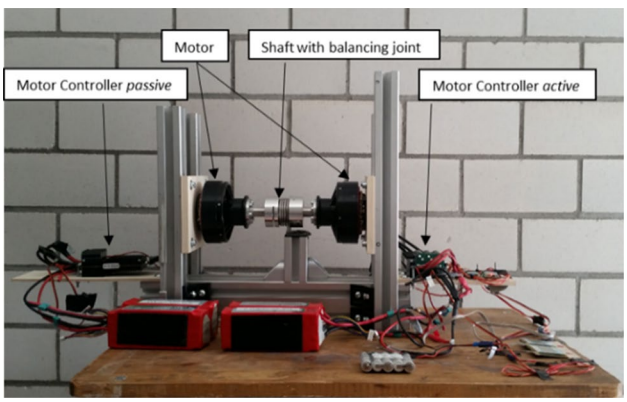

Fig. 29 Windmilling test stand

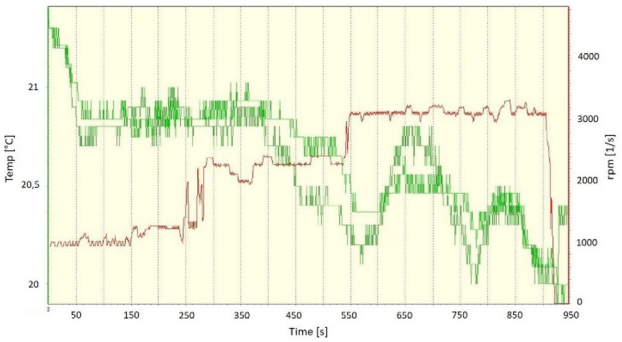

Fig. 30 Temperature and rotation speed of windmilling test

The motor on the passive side is thus mechanically driven as in windmilling and could possibly induce a voltage into the connected motor controller.

For a test of 15 min, the speed is kept at 1000 rpm, 2000 rpm and 3000 rpm for about 5 min each. In the last minute of testing, the battery is unplugged on the passive side to determine to what extent this affects the passive motor controller, since it is missing the massive capacity of the battery. The temperature profiles during the test have been recorded.

The following diagram (Fig. 30) shows the passive side of the experimental setup. The green lines show the temperature profile of the two temperature sensors. During the 15 min test run in windmilling, the temperature of the controller fluctuates between 20 and 21.5 °C. This essentially corresponds to the outside temperature. An unplugged battery on the passive side during the last minute of the test has no measurable effects. The red line represents the speed measurement of the magnetic sensor, which was increased from 1000 to 3000 rpm during the test.

On the passive side, the test simulates the conditions on the motor and motor controller in windmilling. From the test, it could be concluded that the determined temperature profile on the passive side shows no negative effects on the motor controller, whereupon the windmilling can be regarded as uncritical for the motor and the control electronics.

4.3 Provisions for safe operation

As mentioned above, all major changes on the experimental aircraft need to be communicated to the National Airworthiness Authority, the LBA in our case. Together with a detailed description of the changes, an assessment of the effects on the existing structure and systems, including a risk analysis and test results need to be handed in. A brief summary of the most relevant requirements for operation is stated below [13].

– The wingtip propellers must not be used in altitudes below 500 m AGL (above ground level).

- A kill switch must be installed to terminate a propeller runaway.
- The rudder must be capable to compensate the yaw momentum generated by the propellers at all times and flight conditions.
- The structural integrity of the wing must not be compromised by the wingtip pods.
- The aircraft with pods has to be free from flutter within its flight envelope. This has been proven in a dedicated ground vibration test and flutter analysis [14]

5 Ground and flight testing

5.1 Wind tunnel tests

As described in the previous chapter, the tool propcalc [10] has been used to size the powertrain of the wingtip propulsion system. However, the actual thrust generated by the propellers in flow conditions at different speeds has to be verified to ensure safety in case of a one-sided motor runaway. As mentioned before, several safety mechanisms such as a kill switch relay have already been introduced. Nevertheless, safety can be increased if the aircraft is capable of handling the one-sided runaway with the vertical tailplane at any flight speed. This is particularly important, as propeller thrust increases at slower speeds, while at the same time the effectiveness of the vertical tailplane and rudder decreases. Therefore, the capabilities for yaw control of the wtp system and the tailplane need to be investigated at the minimum aircraft speed. This investigation is described in the risk analysis further below since the wtp system needs the calculated power to achieve a comparable yaw control at cruise speed.

The propeller polar generated with the wind tunnel data allows a comparison of the tailplane's yaw control behavior with the wingtip propulsion system in terms of control forces. To process and evaluate the collected data during the flight tests, it is also indispensable to know the propeller efficiency at different flying speeds.

A wind tunnel test has been performed with a completely integrated wingtip pod in a medium-sized low-speed wind tunnel (Göttinger-Type) at the Institute of Aerodynamics and Gas Dynamics of the University of Stuttgart, see Fig. 31.

For the test, the wingtip pod is equipped with a load cell, measuring traction and pressure forces. This load cell is integrated in a movable frame between the electric motor and the pod. In addition, the rotational speed of the propeller, the electric power of the motor and the flow velocity are tracked. Test runs are conducted at different wind tunnel speeds, increasing the rotational speed of the propeller in 500 rpm increments up to the maximum rpm. This set of data allows to derive the polar of the propulsion system for

Fig. 31 Windtunnel test of a wingtip pod

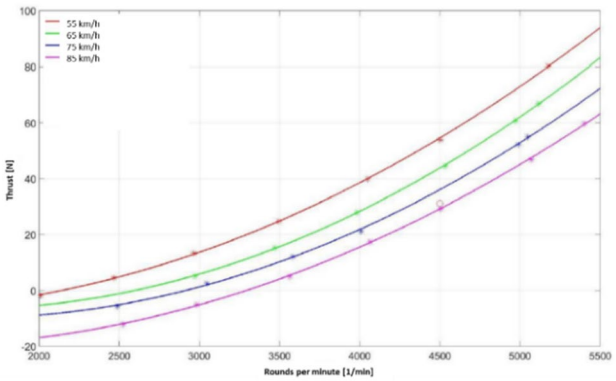

Fig. 32 Thrust vs. rotational speed of wingtip propellers

different speeds (Fig. 32), which is required for processing and evaluating the data logged in flight tests such as yaw angle and yaw rate.

Moreover, a motor brake system was tested in the wind tunnel. The controller of the electric motor was programmed to brake and hold the propeller in position when the propelled yaw control system is not in use. For this test, the flow velocity is increased until the propeller starts to windmill. Furthermore, it was tested up to which flow velocity the electric motor is able to stop the wind milling and to hold the position.

5.2 Flight test procedure

In a first step in the flight test campaign, the wingtip propellers are only tested at altitudes higher than 500 m AGL (Fig. 33). The test program begins with symmetrical flight conditions. The flight range is expanded, stepwise increasing sideslip angles while observing the system behavior. In the event of unexpected system behavior or vibrations, the

Fig. 33 Icaré wtp flight testing

pilot can terminate the test at any time. The flight limitations as laid down in the icaré 2 operating manual are met at all times, also respecting the operational flight envelope.

Each test flight has test objectives clearly formulated and combined in a practicable order for the flight using test cards. A typical pre-flight briefing covers the following topics:

a).Weather.
b).NOTAMS.
c).Airplane configuration.
d).Communication procedures.
e).Test maneuvers including tolerances for speed and altitude.
f).Test objectives.
g).Risks and methods of risk avoidance.
h).Termination criteria.

An example for a standardized test card is shown in Fig. 34.

Testkarte Doubletten

Ziel:	Seitenruder-/wtp-doubletten 55 km/h + 65 km/h	
Datum:		
Flugplatz:		
Startzeit:		
Landezeit:		
Pilot:		
QNH/QFE:		
Wind:		
Frequenz EDTM:	135.180 MHz	1821ft/555m AMSL RW07/25
Frequenz EDPU:	131.115 MHz	2100ft/640m AMSL RW16/34
Frequenz EDST:	125.615 MHz	1167ft/356m AMSL RW13/31
Langen INFORMATION:	128.950 MHz	
Zürich INFORMATION	124.700 MHz	

F-Schlepp/Windenstart oder Eigenstart auf Flughöhe >500m AGL

Getrimmter (Segel-)Geradeausflug	
Angezeigte Eigengeschwindigkeit:	55 km/h ±3km/h
Seitenruderdoublette	einsteuern
Quer- und Seitenruder	neutral
Taumelschwingung	ausschwingen lassen

Getrimmter (Segel-)Geradeausflug	
Angezeigte Eigengeschwindigkeit:	55 km/h ±3km/h
Quer- und Seitenruder	neutral
Poddoublette	einsteuern
Taumelschwingung	ausschwingen lassen

Fig. 34 Icaré wtp flight test card [16]

5.3 Operation modes of the wtp system

The wingtip propellers can be operated in different control modes to use and validate the yaw control abilities.

(a) **Manual mode**
In the manual mode, the pilot can control the wingtip propellers using the additional sidestick (Fig. 7). The x-axis represents a symmetrical control, the y-axis an asymmetrical control. The maximum asymmetry can be triggered with 50% x-axis deflection (stick in the middle) and full y-deflection.

(b) **Asymmetrical thrust proportional to the rudder deflection**
In this mode, the wingtip propellers are automatically controlled directly proportional to the rudder deflection. The pedal position of the rudder is used as a control variable for the wingtip propellers. Thus, in addition to the rudder, these induce a yaw moment and finally a yaw rate. This mode is equivalent to an increasing rudder efficiency. This control mode is referred to as "rudder mode".

(iii) **Asymmetrical thrust proportional to the aileron deflection**

Another mode for controlling the wingtip propellers is an automatic control via the aileron deflection. The y-position of the stick, which corresponds directly to the aileron deflection, is used as a control variable for the wingtip propellers. This mode reduces the very pronounced roll-yaw momentum of the icaré 2 and thus reduces the coupling between the x- and z- axes of the aircraft. This allows for more coordinated, sliding-free curves without using the rudder. This control mode is referred to as "aileron mode".

(iv) **Automatic doublettes**

An automatic doublette induced by the wingtip propellers was introduced to generate comparable test data. It can be triggered automatically by a button on the sidestick. A time constant of two seconds was chosen for the doublette. First the full power is applied on the right propeller for 2 s, followed by 2 s of full power on the left propeller. Thus, the excitation of the aircraft (input signal) is always the

same and thus the output in terms of rotation rates, Euler angles, sliding angles can be compared.

(e) **Automatic control of the angle of sideslip**

The wingtip propellers can also be controlled respecting a pre-set angle of sideslip (beta). This automatic mode is independent of pilot inputs via the stick. The gain, i.e. the gain of the closed control loop, can be controlled via a potentiometer on the sidestick.

The aim of the sideslip angle control mode is to keep the beta angle at zero which is measured by the air data boom. This control mode is referred to as "beta mode".

5.4 Flight test maneuvers

For the icaré 2 wtp flight test campaign, a number of maneuvers has been identified which are highly suitable to validate the capabilities of the wingtip propellers in terms of yaw control.

a) **Jump/step input signal**

Jump inputs are short but distinct maneuvers. They can be entered via rudder, aileron, elevator or thrust. Such maneuvers are followed by a response of the system, the step response, allowing for determining the system transfer function and characteristics. Elevator jump inputs can be used, for example, to stimulate a phugoid.

b) **Doublettes**

Doublettes are symmetrical rudder deflections starting from the rudder neutral position, consisting of a defined deflection in one direction, followed by a defined deflection in the opposite direction. Elevator doublettes are suitable to stimulate an angle of attack oscillation without stimulating a phugoid. Rudder doublettes can be conducted to stimulate a dutch-roll.

Due to their wide frequency spectrum, doublettes can also be used for parameter identification in the time domain. Different time constants and amplitudes can be used to generate a desired power density distribution in the frequency domain.

iii) **Chirp signal**

The chirp signal is a sinusoidal signal with increasing frequency. The resulting wide frequency spectrum enables parameter identification in the frequency range [17]. The start and end frequencies can be adjusted depending on the area of interest. In a flight test, the chirp signal must be activated manually and is therefore subject to fluctuations.

iv) **Roll exercises**

Roll exercises are used in glider pilot training to practice coordinated aileron and rudder deflections. The aircraft is aligned to a point on the horizon and alternating roll angles between 20° and 30° are flown with symmetric deflection of ailerons and rudder.

The roll-yaw momentum must be balanced with the rudder so that the nose of the aircraft remains aligned to the previously defined point. In case of a strong coupling of the roll-yaw momentum (as it is the case for the icaré 2), it is recommended to deflect the rudder ahead of the aileron.

Roll inputs without rudder compensation lead to considerable angles of sideslip. The wingtip propellers are used in lieu of the rudder to generate the yaw momentum required for compensation.

e) **Compensation of the differential wingtip propeller thrust with the rudder**

The wingtip propellers are a secondary control unit for generating a yaw momentum. For a comparison of the control authority, symmetrical maneuvers are flown, in which the yaw moment of the wingtip propellers is compensated with the rudder at different speeds. It is to be noted that the rudder effectiveness increases with higher airspeed, while the yaw moment, which can be generated by the wingtip propellers, decreases with increasing airspeed.

5.5 Risk analysis

The risk analysis lists (Fig. 35) conceive failures and operating errors and, where available, offer a method for minimizing the effects and hazards. Each test method and the possible failure cases are assessed with a probability of occurrence and an extent of damage. A risk matrix (Fig. 36) combines probability of occurrence and the hazard potential. It can be used to determine whether the risk is too high, or where risk mitigation measures should be taken.

In case of the wingtip propulsion system, ground tests and simulations helped to investigate the probability of occurrence and the hazard potential. The capabilities for yaw control of the wtp system and the tailplane need to be investigated at the minimum aircraft speed because of the contrary behavior of propeller thrust and control surface authority. The windtunnel test of the wingtip propeller yield a thrust of.

$T = 80N$ at the minimum speed.

$v_{min} = 16m/s$.

This results in $M_{z,wtp} = 936Nm$.

As for the sizing of the wtp system for the cruise speed, the theoretical approach according to DATCOM [8] and a

Failure	Risk value	Risk minimization strategy
Maximum asymmetric thrust	6	Wingtip propellers only activated 500m AGL. Simulations with maxium assymmetrical thrust, showing controllability with the rudder.
Structural overload due to flutter	4	Ground vibration testing & flutter analysis have been conducted. Flutter is not critical for the low test speeds. First flights flown without wingtip propellers in order to collect data and keep the vibration input as low as possible.
Failure of main engine	2	Airplane to be flown as a glider and operated accordingly.
Main battery fire	8	Depending on the severity, the pilot has various options: - land as quickly as possible, also outside of an aerodrome, - remove hood (smoke exhaust), - parachute exit.
Wingtip pod battery fire	6	Land as quickly as possible, also outside of an aerodrome.
Flow interference of aileron and wingtip propeller	4	Limit size of wingtip propellers.
Transition to spin due to high angles of sideslip	4	Spin recovery with aileron neutral and rudder against spin direction.

Fig. 35 Examples for failures and risk minimization strategies [15]

Probability of occurence \ Damage	negligible (1)	marginal (2)	hazardous (3)	catastrophic (4)
very low (1)	1	2	3	4
low (2)	2	4	6	8
medium (3)	3	6	9	12
high (4)	4	8	12	16

Fig. 36 Risk matrix for icaré wtp flight testing [14]

FlightStream® [9] simulation have been conducted for v_{min} to compare with $M_{z,wtp}$ at v_{min} and to evaluate if an asymmetrical wtp runaway is of high risk for slow flying speeds for example during landing. The following results has been determined, respectively, simulated.

$$M_{z,DATCOM}(27°) = 931\text{Nm}$$

$$M_{z,FlightStream®}(27°) = 706\text{Nm}$$

When using the maximum rudder deflection, both results are lower than the $M_{z,wtp}$ which leads to a safe operation at the minimum speed. Hence, the asymmetric wtp runaway can be compensated immediately by a pilot reaction on the rudder leaving very little time for an uncontrolled flight condition.

6 Conclusion and outlook

Wingtip propellers have been installed as a primary flight control system on the icaré wtp. The development, manufacturing and sizing of the pods suits the requirements of the aircraft. The pods can be detached easily for maintenance, battery charging and to use the icaré for flight tests in the normal configuration. Around 25 h of test flights have been conducted to date with wingtip propellers in several modes and configurations. These tests showed an adequate sizing of motor, propeller, motor controller and battery, avoiding overheating or over currents. As predicted in the sizing calculations, the effectiveness of the wing tip propellers is adequate to generate sufficient yaw momentum to replace the rudder. Finally, the identified risks showed to be very unlikely and the risk mitigation strategies proved to be suitable.

Further testing with different configurations is planned for the next flight test campaigns. Folding propellers are in development to increase the feasible propeller diameter which is limited for fixed propellers due to the ground clearance (see Fig. 23). In the Lufo project ELFLEAN, a 33.3% model of the electric [18], now hybrid-electric [19], manned research aircraft e-Genius—the e-Genius Mod [20]—designed, built, and operated at the University of Stuttgart—is currently used to investigate the aerodynamic effects of wing tip propellers [21]. The e-Genius Mod wingtip pods additionally have a load

cell to measure the thrust the wing tip propeller generates. This setup allows to measure the effect on the induced drag and to evaluate overall aircraft performance and energy consumption of the wtp propulsion system compared to the use of a rudder [22]. Performance results of a wingtip propulsion system at the e-Genius 1:3 model are published in Pfeifle et al. *"Verifying the Effect of Wingtip Propellers on Drag Through In-Flight Measurements"* [23]. A similar setup could be implemented in the wingtip pods of the icaré wtp to measure the thrust and to also evaluate the aerodynamic effects.

Acknowledgements The authors would like to thank the Flugplatz Mengen-Hohentengen GmbH for the good cooperation during the flight test campaign.

Funding Open Access funding enabled and organized by Projekt DEAL.

References

1. Schmollgruber, P., Donjat, D., Ridel, M., Cafarelli, I., Atinault, O., François, C., Paluch, B.: Multidisciplinary design and performance of the ONERA Hybrid Electric Distributed Propulsion concept (DRAGON). January 2020. AIAA Scitech Forum.
2. Hepperle, M.: Aspects of distributed payload a view on regional aircraft. Stuttgart, 19. Februar 2016. Symposium elektrisches Fliegen.
3. Kim, H.D., Perry, A.T., Ansell, J.P.: A review of distributed electric propulsion concepts for air vehicle technology. Cincinnati (2018)
4. Mangold, J., Lang, M., Stober, J., Ladwein, F., Will, F.: NASA/DLR Design Challenge 2019. HyBird Aircraft Concept Final Report. Stuttgart, 01 July (2019)
5. Borer, N.K. et al.: Comparison of aero-propulsive performance predictions for distributed propulsion configurations. AIAA SciTech Forum. 55th AIAA Aerospace Sciences Meeting. 2017, S. 246. ISBN 978-1-62410-447-3.
6. Borer, N.K., Patterson, M.D., Viken, J.K., Moore, M.D., Bevirt, J., Stoll, A.M., Gibson, A.R.: Design and performance of the NASA SCEPTOR distributed electric propulsion flight demonstrator. In: AIAA Aviation Technology, Integration, and Operations Conference June (2016)
7. Miranda, L., Brennan, J.: Aerodynamic effects of wingtip-mounted propellers and turbines. In: 4th Applied Aerodynamics Conference Virginia June (2012)
8. Hoak, D.E., et al.: USAF stability and control Datcom. Flight Control Division, Air Force Flight Dynamics Laboratory. WPAFB, Ohio 1978, revised
9. Roskam J. Airplane design Part VI: Preliminary calculation of aerodynamic, thrust and power characteristics. Kansas (1987)
10. Wortmann FX. Symmetrical airfoils optimized for small flap deflection. Stuttgart
11. Research in Flight. Flightstream® Vorticity Flow Solver. https://researchinflight.com/. Last Accessed Feb 2021
12. Schenk H. Die Zusammenarbeit von Propeller und Elektromotor. http://www.drivecalc.de/PropCalc/PCHelp/Prop+Motor.pdf Last Accessed Mai 2022
13. Hacker Motor GmbH. https://www.hacker-motor.com/. Last Accessed Feb 2021
14. Xoar International llc. https://www.xoarintl.com/. Last Accessed Feb 2021
15. Pfeifle, O., Frangenberg, M., Notter, S., Denzel, J., Bergmann, D.P., Schneider, J., Scholz, W., Fichter, W., Strohmayer, A.: Distributed electric propulsion for yaw control: testbeds, control approach, and flight testing. AIAA 2021–3192. AIAA Aviat. 2021 Forum (2021). https://doi.org/10.2514/6.2021-3192
16. Strohmayer, A.: Vorhabenbeschreibung: icaré2 mit Randpropeller. Stuttgart (2018)
17. Chaiec, W., Krzymien, W., Strohmayer, A.: The effect of wingtip propulsors on Icaré aeroelasticity. Aircr Eng Aerosp Technol (2017). https://doi.org/10.1108/AEAT-12-2017-0279
18. Sturm M. Erprobung und Bewertung von Flächenendpropellern am Icaré 2 wtp. Master thesis, Stuttgart, October (2019)
19. Tischler, M.B., Remple, R.K.: Aircraft and rotorcraft system identification—engineering methods with flight-test examples, AIAA Education Series (2006)
20. Geiß, I., Notter, S., Strohmayer, A., Fichter, W.: Optimized operation strategies for serial hybrid-electric aircraft. In: Aviation Technology, Integration, and Operations Conference (2018)
21. Geiß, I., Voit-Nitschmann, R.: Sizing of the energy storage system of hybrid-electric aircraft in general aviation. CEAS Aeronaut. J. **8**(1), 53–65 (2016)
22. Bergmann, D.P., Denzel, J., Baden, A., Kugler, L., Strohmayer, A.: Innovative scaled test platform e-genius-mod—scaling methods and systems design. Aerospace **6**(2), 20 (2019)
23. Bergmann, D.P., Denzel, J., Pfeifle, O., Notter, S., Fichter, W., Strohmayer, A.: In-flight lift and drag estimation of an unmanned propeller-driven aircraft. Aerospace **8**(2), 43 (2021). https://doi.org/10.3390/aerospace8020043
24. Pfeifle, O., Fichter, W., Bergmann, D.P., Denzel, J., Strohmayer, A., Schollenberger, M., Lutz, T.: Precision performance measurements of fixed-wing aircraft with wing tip propellers. AIAA Aviat. (2019). https://doi.org/10.2514/6.2019-3088
25. Pfeifle, O., Notter, S., Fichter, W., Bergmann, D.P., Denzel, J., Strohmayer, A.: Verifying the effect of wingtip propellers, on drag through in-flight measurements. J. Aircr. (2021). https://doi.org/10.2514/1.C036490